RHEOLOGICAL ASSESSMENT OF NEAT PAVING, AIR RECTIFIED PAVING AND OXIDIZED ROOFING BITUMEN

Pavel Kriz[1], John H Brownie[1], Alan G Blahey[1], Katherine L Sokol[1], Daniel L Grant[1], Frédérique Cointe[2], Nadjib Boussad[3], Ralph D Shirts[4]

[1]Imperial Oil Research Centre, 453 Christina St. S., Sarnia, ON N7T 8C8, Canada
[2]Esso S.A.F., Tour Manhattan, La Défense 2, 5/6 place de l'Iris, 92400 Courbevoie, France
[3]Esso S.A.F., European Technology Centre, B.P.37 - Porte Saint Georges, 76330 Notre Dame de Gravenchon, France
[4]ExxonMobil Corp., 3225 Gallows Road, Fairfax, VA, 22037, USA

ABSTRACT

The objective of this study was to provide a detailed rheological analysis of neat, air rectified and oxidized bitumen in order to understand the impact of severity of oxidation on their rheological behavior as compared to traditional empirical testing methodologies. Two straight-run bitumen feedstocks, PG 64-22 and PG 46-34, were air blown to varying degrees at three different temperatures. Air blown products, ranging from air rectified paving grades to oxidized Built-Up Roofing Bitumen Type III, were produced and subjected to detailed rheological analysis.

Dynamic material functions were obtained and merged into mastercurves and analyzed. Relaxation and retardation spectra were calculated, and relaxation modulus and creep compliance functional dependencies in the time domain were derived. It was determined that the steady-state compliance shows differences for air rectified and oxidized bitumen.

As a general trend, oxidation increased bitumen modulus, viscosity and relaxation times. The impact of oxidation on relaxation properties was the most significant. All bitumen, despite the severity of oxidization, exhibited behavior similar to low molecular weight uncross-linked polymer, confirming no dramatic change in molecular weight and no true cross linking among bitumen molecules take place during air blowing. It is suggested, that the changes in material properties predominantly arose from increased rigidity of molecular chains (aromatization, de-saturation), higher tendency for weak intra-molecular associations (increased polarity) and possibly phase separation.

Traditional parameters such as penetration index or penetration viscosity number are shown to trend well with scientific rheological parameters when severity of oxidation is considered.

Keywords: Temperature Susceptibility, Rheology, Ageing, Complex Modulus, Zero Shear Viscosity

1. INTRODUCTION

The objective of this study was to understand the effect of oxidation severity on the rheological behavior of bitumen. During air blowing, the bitumen composition is altered by chemical reactions in the presence of oxygen. These compositional changes are primarily due to dehydrogenation, aromatization, introduction of oxygen containing polar functional groups, etc. [1]. Minor changes to composition may also arise from evaporation at the process temperatures. Rheology can be used to study the impact of these changes on bitumen properties and performance.

This work examined the rheology of a series of bitumen samples including neat, air rectified and oxidized bitumen. Small strain amplitude oscillatory testing with mastercurve analysis was used to evaluate the rheological properties of the bitumen materials. A number of oscillatory frequency sweeps was performed over a broad range of constant temperatures. The individual data sets were then merged into a single mastercurve using the Time-Temperature Superposition principle (TTS). The mastercurves represent a continuous material function over a broad temperature and time or frequency domain, therefore represent a 'library' of rheological parameters which can be readily derived or calculated at any desired temperature, loading time or frequency.

2. MATERIALS AND METHODS

Two straight-run bitumen samples were manufactured from 100% Cold Lake Blend crude oil feedstock at the Imperial Oil Strathcona Refinery. The samples, identified as PG 64-22 (PAVE) and PG 46-34 (roofing bitumen flux, RAF) were laboratory air blown at 200, 230, and 260 °C to produce a range of air rectified and oxidized products. These feedstocks were specifically selected because they have widespread commercial use in road and roofing applications. The variability associated with chemical composition was minimized by using consistent Cold Lake Blend bitumen, so that measured changes in rheological performance may be more precisely related to the effect of oxidation alone. All air blown samples (air rectified and oxidized) were prepared at the Imperial Oil Ltd. Sarnia Research Centre (SRC) except RAF-210-15 which was prepared at the Esso S.A.F. European Technical Centre (ETC) for comparison purposes. Sample details, including physical properties, are presented in Table 1. For process conditions see Table 2. Pfeiffer Penetration Index (PI) was calculated as $PI = 20(1-25A)/(1+50A)$, where $A = (\log PE25 - \log 800)/(25 - SP)$, and where $PE25$ is bitumen penetration at 25 °C and SP is the softening point [2].

Table 1. Samples subjected to rheological testing.

Sample ID*	Oxidation temperature, °C	Oxidation time, min	Pen. at 25 °C, 100g/5s, dmm	Softening point, °C	Pfeiffer Penetration Index
RAF	-	0	360	32	-1.4
PAVE	-	0	92	43.8	-1.4
RAF-220-18	260	220	18	90	3.3
RAF-90-74	260	90	74	50	-0.2
RAF-170-25	260	170	25	74	1.9
RAF-210-15**	260	210	15	96.2	3.6
PAVE-145-18	260	145	18	81.1	2.2
PAVE-30-59	260	30	59	49.3	-1.0
RAF-295-20	230	295	20	93.1	3.8
RAF-110-62	230	110	62	52.2	-0.1
RAF-220-31	230	220	31	72.4	2.1
PAVE-40-60	230	40	60	49.6	-0.9
PAVE-350-14	230	350	14	90.2	2.8
RAF-460-22	200	460	22	89.9	3.7
RAF-170-60	200	170	60	54.1	0.3
RAF-340-32	200	340	32	72.7	2.2
PAVE-90-51	200	90	51	51.8	-0.7
PAVE-450-16	200	450	16	86.6	2.6

*) Nomenclature for Sample ID: Feedstock (PAVE for PG 64-22, RAF for Roofing Bitumen Flux) – Oxidation time in minutes – Penetration in dmm.
**) Air blown at Esso S.A.F. European Technical Centre (ETC). All remaining samples air blown at Imperial Oil Research Centre (SRC).

A Thermal Analysis (TA) AR 2000ex rheometer equipped with a liquid nitrogen cooling system was used for small strain dynamic oscillatory testing. Parallel plate geometry was used in all tests. Gap settings and typical plate diameter selection are listed in Table 3. The minimum test temperature ranged from −10 to 0 °C, depending on sample stiffness and brittleness. The maximum test temperature varied according to sample stiffness and ranged between 60 °C (RAF) and 130-150 °C (BURA III). The temperature increment for isothermal tests was 10 °C. A strain sweep was performed at 100 rad/s for each test temperature and each sample category (i.e. straight-run, air rectified, and oxidized grades) to determine the linear viscoelastic region and appropriate strain level for subsequent frequency sweeps. Dynamic oscillatory frequency sweeps were performed from 0.1 to 100 rad/s at each temperature. Mastercurves were merged graphically in the TA Data Analysis software. The reference temperature was 30 °C. Mastercurves were obtained for the material functions $G'(\omega), G''(\omega)$.

Table 2. Process Conditions in SRC and ETC Oxidizer

Air rate	Pressure	Mixer rpm	Batch size	Oxidation time and temperature
50 L/kg/hr	Atmospheric	SRC 1800, ETC 520	3 L	See Table 1

Table 3. Geometry, temperature ranges and gap settings.

Geometry – typical for asphalts	Temperature*	Gap
40 mm Parallel plate	50 (90) to 70 (150) °C	0.5 mm
25 mm Parallel plate	20 (50) to 50 (90) °C	1 mm
8 mm Parallel plate	−10 (0) to 20 (50)°C	2 mm

*) typical test temperature range for soft samples, i.e. RAF; and stiffest, i.e. BURA III in brackets.

3. RESULTS AND DISCUSSION

3.1   Material Functions $G'(\omega), G''(\omega)$

In a sinusoidal deformation process, the storage modulus, G', is defined as the stress in phase with the strain divided by the strain; it is a measure of the energy stored and recovered per cycle. Storage modulus represents the "in-phase" component of complex modulus and it is a measure of a material's elastic response to applied strain. Storage modulus as a function of reduced frequency is presented in Figure 1A. For simplicity, results are shown for samples air blown at 260 °C only, since they are representative of air blowing data at 200 and 230 °C.
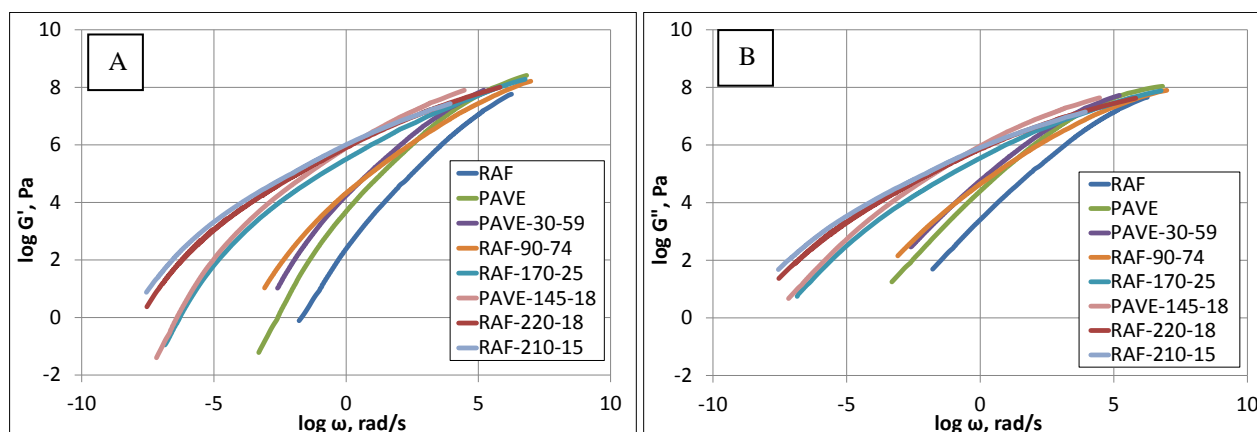
Figure 1. Storage modulus versus reduced frequency (A). Loss modulus versus reduced frequency (B).

The loss modulus, G'', is defined as the stress component 90° out of phase with the strain divided by the strain; it is a measure of the energy dissipated or lost as heat per cycle of sinusoidal deformation. It represents the "out-of-phase" component of complex modulus and is a measure of material viscous response during sinusoidal deformation.

At high frequencies, where the material response is mostly elastic, little stress relaxation takes place and comparatively little energy is dissipated in periodic deformations. Therefore, $G''(\omega)$ tends to be considerably lower than $G'(\omega)$ in this frequency zone (Figure 1B). Regardless of oxidation temperature, the storage modulus of all bitumen samples asymptotically approached a value of ~10^9 Pa, which represents the approximate modulus of bitumen glass. Molecular mobility is greatly reduced in the high frequency zone, and large scale molecular rearrangements do not occur within the experimental time frame. Storage modulus in the high frequency region slightly increased with degree of oxidation and was also slightly higher for PAVE and PAVE oxidized samples than for comparable RAF counterparts. This observation will be discussed further in Section 3.2.

At low frequencies, the storage modulus fell rapidly in all samples. This zone is typically referred to as terminal. The modulus in the terminal zone dropped in a single stage, i.e. no plateau was observed. This is an indication that there are no cross-links created during bitumen oxidation. Bitumen mean molecular weight would have to significantly increase if cross-linking takes place during oxidation. It was reported that molecular weight does not increase dramatically during bitumen oxidation [1]. Moreover, in uncross-linked polymers, the loss modulus at very low frequencies should exhibit direct proportionality of G'' to ω or a slope of one on a logarithmic plot [3]. This relationship was observed for all bitumen samples examined in this work, providing further evidence that true (σ-bond) crosslinking is unlikely to occur during bitumen oxidation.

A major change observed with increased oxidation time was that the storage and loss modulus curves shifted to lower frequencies. This can be explained in molecular terms. For uncross-linked polymers, such a shift is generally attributed to an increase in molecular weight and/or an increase in the number and length of side chains. Additionally, an increase

in polymeric chain rigidity and reduction in mobility by the introduction of multiple bonds or crosslinking can result in a similar effect [4]. During bitumen oxidation, side chain cleavage typically occurs, and the mean molecular weight has been reported not to increase dramatically if at all [1]. Thus, an increase in side chain number and length or an increase in molecular weight cannot explain the modulus increase of several orders of magnitude observed here. As cross-linking was already excluded, the increase of storage modulus must therefore result from increased rigidity and reduced mobility of molecular structures and possibly from increased tendency of intra-molecular associations.

The impact of oxidation on molecular mobility of bitumen can be explained by following analogy to polymer chemistry. As reported by van Krevelen [5,6], polymer glass transition temperature can be accurately calculated by simply adding a contribution of each functional group to the overall glass transition temperature. Each functional group has constant partial glass transition temperature, T_{gi}. Glass transition temperature is inversely related to molecular mobility, i.e. the higher the mobility the lower the glass transition temperature. Generally, saturated and linear functional groups have high molecular mobility due to the rotational degree of freedom of the single bond and very low T_{gi}. Aromatic rings, unsaturated chains, as well as oxidized functional groups omit the rotational degree of freedom of a single covalent bond have high T_{gi} and reduce overall molecular mobility. The major reactions during asphalt oxidation are dehydrogenation (unsaturation), aromatization (ring closure), side chain scission (loss of saturated chains) etc. Carbonyl and sulphonyl groups are also common products of bitumen oxidation [7]. All these reactions lead to gradual replacement of highly mobile saturated functional groups by unsaturated, aromatic or oxidized heteroatom functional groups of very low mobility. The overall molecular mobility thus reduces with oxidation. The changes are rather significant. For instance, T_{gi}, of the carbonyl group (C=O, product of oxidation) is 964 K, while T_{gi} of the ether group (C-O-C) is 232 K. The presence of sulfur in the chain (C–S–C, T_{gi} of 234 K) may lower the overall glass transition temperature while T_{gi} of the SO_2 group (905 K) may do the opposite. The observed increase of moduli with severity of oxidation can be primarily attributed to reduced molecular mobility and increased molecular rigidity. The intra-molecular associations may also contribute to modulus increase as it is discussed further in Section 3.3.

3.2   Loss Tangent, $\tan\delta$

The loss tangent is a dimensionless parameter which represents the ratio of energy lost to energy stored in a cyclic deformation, $\tan\delta = G''/G'$. Loss tangent can also be thought of as an index of viscoelasticity. Since the phase angle, δ, can range from 0° for perfectly elastic solids to 90° for purely Newtonian liquids, the loss tangent correspondingly ranges between zero and infinity, with smaller values representing a more elastic material response.

For higher frequencies, the experimental data revealed that the loss tangent decreased with increased oxidation time. Thus, the bitumen became more elastic with increased oxidation severity (Figure 2A). Loss tangent of the PAVE and PAVE air blown samples also decreased at a steeper slope in the glassy zone compared to that for the RAF counterparts. This observation is explained by recognizing that the PAVE sample is a deeper distillation cut and omits a fraction of lower boiling molecules present in the RAF sample. These molecules are mostly saturated, highly mobile and relatively indifferent to oxidation, and although these molecules may be partially evaporated during air blowing, they remain largely unchanged in structure in the RAF air blown samples. As the glassy zone is approached, therefore, these molecules are the most mobile and contribute to stress relaxation and viscous response of the material. Thus, the loss tangent in the glassy zone is higher in the RAF samples versus their equivalent PAVE counterparts.

At medium frequencies, the loss tangent and the slope of the loss tangent decreased with the oxidation time at any given frequency. This supports empirical observations that temperature susceptibility decreases with oxidation severity. The air blown samples retain a higher degree of elasticity at a given frequency. In terms of molecular mobility, oxidized molecules need a longer time (lower frequency) to relax imposed stresses. The larger plateau in the air blown samples also indicates a much wider distribution of molecular mobilities, especially for the RAF air blown samples. This observation is consistent with previous analysis. For low frequencies, the loss tangent gradually increases and eventually becomes inversely proportional to frequency. All samples followed this trend, which is also typical behavior for low molecular weight uncross-linked polymers (M_w ~ 10,000 g/mol) as they reach the terminal zone.

3.3   Dynamic viscosity, $\eta'(\omega)$

The real component of complex viscosity, often called dynamic viscosity, is useful in describing the behavior of the uncross-linked systems. The dynamic viscosity as a function of reduced frequency is presented in Figure 2B. At very low frequencies, the dynamic viscosity of all samples simply approached the steady-flow viscosity, η. This is typically observed for uncross-linked polymers and confirms that there is no true crosslinking present in even the most oxidized samples. The asymptotic viscosity value at low frequency increased with oxidation severity, and lower molecular mobility in the air blown samples is one of the major reasons for this observation. At very low frequencies (or high temperatures), however other factors may also be important. Reactions, typically seen during oxidation such as dehydrogenation, aromatization or functional group oxidation increase the capacity for weak molecular forces. Inter- and intra-molecular forces typically observed among bitumen molecules are charge transfer forces, electrostatic interactions, van der Waals interaction, exchange-repulsion interaction, forces arising from induced dipole, and

hydrogen bonding [8-11]. The association energies between the most polar molecules are on the order of 5 kJ/mol [12] while single covalent bonds (true cross-links in polymers) are much stronger; typically on the order of 180−450 kJ/mol [13]. Inter- and intra-molecular interactions are promoted with increasing polarity of bitumen constituents (oxidation time). Weak interactions further limit the molecular mobility and may promote the formation of relatively stable molecular aggregates of significantly higher apparent molecular weight, or they may eventually lead to phase separation.
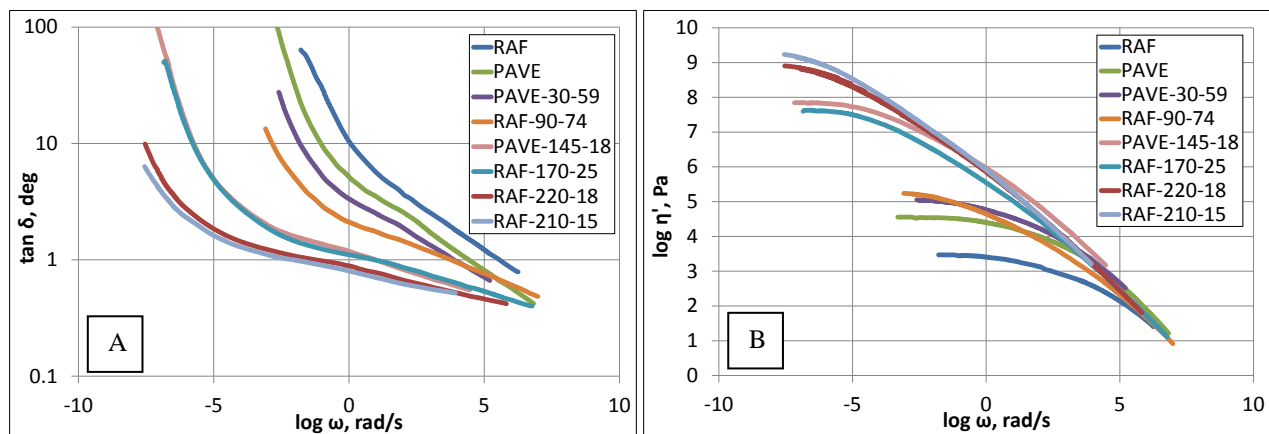

Figure 2. Loss tangent versus reduced frequency (A). Dynamic viscosity versus reduced frequency (B).

3.4 Black Diagram, $G^*(\delta)$

Plotting the material functions in a black diagram is a useful technique to visualize the rheological characteristics (fingerprint) of a material. The black diagram is presented in Figure 3A. Each point in black space represents a common frequency, thus the position of the material function on the frequency or time scale is irrelevant to this plot. Neat bitumen samples (PAVE and RAF) originating from the same crude oil were found to form identical curves in the black diagram regardless of the fact that they may possess very different penetrations (92 versus 360 dmm). The material functions, $G'(\omega), G''(\omega)$, of neat bitumen have identical shape and are only shifted along the time scale as their penetration changes. This observation can be explained as follows. The neat bitumen samples are identical in terms of molecules which have the greatest impact on material viscoelasticity (asphaltenes and resins) with the softer bitumen being only a more 'diluted' form. As frequency is irrelevant in the black space, the neat samples essentially appear identical in this plot, despite each common point corresponds to a different frequency. Therefore, the black diagram can screen out the contribution of the saturated ('diluent') molecules. As the non-polar, saturated molecules undergo little change during oxidation, the black diagram is shown here to be very useful in separating the fundamental changes in bitumen molecular composition due to oxidation from distillation or evaporation.
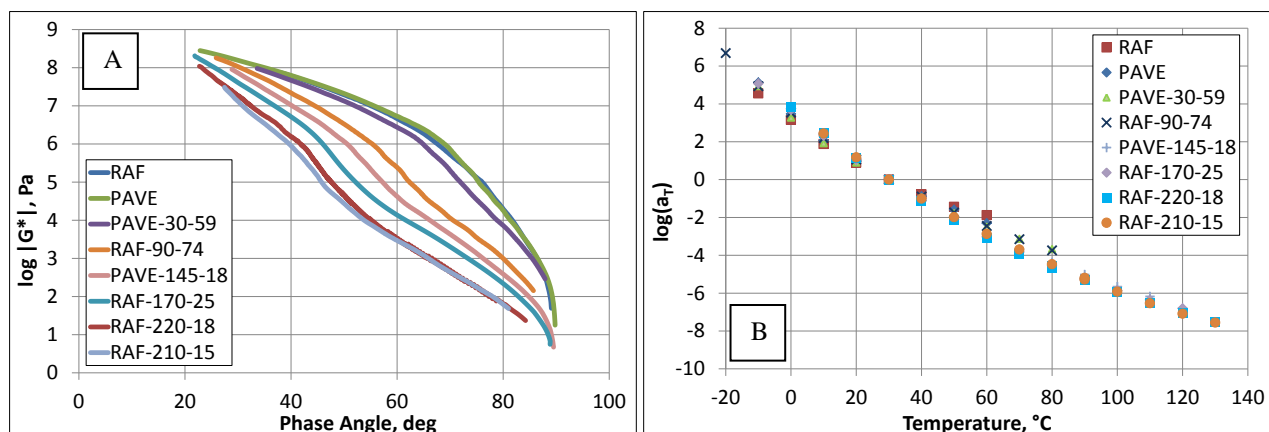

Figure 3. Black diagram (A). Horizontal shift factors versus temperature (B).

Short air rectification of PAVE samples to 50/70 paving grade showed similar black diagram shapes as those for neat bitumen. This suggests that the chemical structure or character was not significantly altered in these samples. With increased oxidation time, the deviation from an initial shape of neat bitumen gradually progressed, indicating a change in molecular structure and composition. The oxidation time at a given temperature was found to be the most important factor influencing curve shape progression in the black diagram, while feedstock penetration does not seem to be a factor.

An inflection point in the black diagram at $|G^*| \cong 10^5 \text{Pa}$ was observed for more oxidized samples (all remaining samples except RAF, PAVE and air rectified paving grade originated from PAVE). This may be an indication of phase separation. Oxidation primarily alters polar molecules and to a lesser extent the remaining aromatics. Saturated molecules remain largely unaltered during oxidation, as they are the most stable. Therefore, the polarity of the polar molecules increases faster than the polarity of the remaining bitumen constituents during oxidation. In terms of solubility, the decrease in solubility of the most polar molecules is possibly faster than the increase in solvent power of the remaining molecules. This difference may result in phase separation. Additional analysis, such as modulated differential scanning calorimetry [14] may provide an additional insight into the phase stability of air blown bitumen.

3.5 Time - Temperature Domain Transformation

The time-temperature superposition principle can only be applied for thermorheologically simple materials and within the limits of linear viscoelasticity. The relaxation time, $\tau_i(T)$, at temperature T is simply related to the relaxation time, $\tau_i(T_r)$, at an arbitrarily chosen reference temperature, T_r, via the relationship $a_T(T,T_r) = \tau_i(T)/\tau_i(T_r)$, where a_T is a horizontal shift factor. The horizontal shift factor is therefore associated with the temperature dependence of the relaxation time [3]. A horizontal shift factor, a_T, for each isotherm with respect to reference temperature (30 °C) was obtained for each test temperature (Figure 3B). When a functional relationship is found for the horizontal shift factors as a function of the temperature, the domain of the material functions can be transformed from frequency to temperature. For temperatures above the glass transition temperature, T_g, the Williams-Landel-Ferry (WLF) model [15] typically provides a good fit of the experimental data:

$$a_T(T,T_r) = -\frac{C_1(T-T_r)}{C_2+T-T_r} \qquad \textbf{1}$$

where C_1, C_2 are the empirical fitting parameters. Now the frequency domain (ω) of the mastercurve can be converted to the temperature domain for an arbitrarily selected testing frequency (ω_t).

$$T = T_r + \frac{C_2 \log(\omega_t/\omega)}{C_1 + \log(\omega/\omega_t)} \qquad \textbf{2}$$

In order to verify the mastercurve data, the parameter $G^*/\sin\delta$ was calculated as a function of temperature at constant testing frequency of 10 rad/s (selected to be the frequency specified in AASHTO T315 standard). A temperature, where $G^*/\sin\delta$ equals 1 kPa was calculated for each sample. This result was compared to a true high temperature performance grade calculated from a dynamic shear rheometer test as per AASHTO T315 method at pass and fail temperature. A very good correlation was achieved between the mastercurve results and the standard AASHTO T315 test results, confirming the applicability of the merging process and the WLF model for bitumen (Table 4). Validation of mastercurve construction and WLF model application is critical in order to accurately compare the results for various samples and ties the mastercurve results back to a standard testing methodology.

3.6 Christensen-Anderson-Marastenau Model (CAM)

Christensen-Anderson (CA) model was developed during the Strategic Highway Research Program [16] to describe a bitumen mastercurves with three parameters. These parameters can eventually be obtained from standard AASHTO asphalt test results without a need for complete mastercurves dataset. The model parameters can subsequently be used to predict the rheological properties of road mixtures allowing for rapid screening without lengthy laboratory testing. The CA model introduced a set of two equations for G^* and δ:

$$\log G_r(\omega) = -\frac{R}{\log 2} \log\left[1 + \left(\frac{\omega}{\omega_0}\right)^{-\frac{\log 2}{R}}\right] \qquad \textbf{3}$$

$$\delta(\omega) = \frac{\pi}{2}\left[1 + \left(\frac{\omega}{\omega_0}\right)^{\frac{\log 2}{R}}\right]^{-1} \qquad \textbf{4}$$

where $G_r(\omega)$ is the reduced modulus; $G_r(\omega) = G^*(\omega)/G_g$, G_g is the glassy modulus, $\delta(\omega)$ is the phase angle, ω is the reduced frequency, ω_0 is the crossover frequency, $\omega_0 = 1/\tau_m$, where τ_m is the mean relaxation time and R is the rheological index associated with the width of the relaxation spectrum. In order to further improve the CA model, an adjusting parameter, κ, was added to the model by Marasteanu; Christensen-Anderson-Marasteanu model or CAM model [17]:

$$\log G_r(\omega) = -\frac{\kappa}{\beta} \log \left[1 + \left(\frac{\omega}{\omega_0} \right)^{-\beta} \right] \qquad \qquad \textbf{5}$$

$$\delta(\omega) = \frac{\pi}{2} \kappa \left[1 + \left(\frac{\omega}{\omega_0} \right)^{\beta} \right]^{-1} \qquad \qquad \textbf{6}$$

Where β is the relaxation spectrum width parameter, $\beta = (\log 2)/R$. The adjusting parameter κ is associated to the convergence velocity of the phase angle data to asymptotic values from 0 to 90 degrees.

Table 4. Comparison of DSRo limiting temperature – standard AASHTO T315 and calculated values from mastercurves (WLF transformation).

Sample/Method	DSRo, T at 1.00 kPa M320, °C	DSRo, T at 1.00 kPa Mastercurve, °C	Δ, °C
PAVE	64.4	64.3	0.1
PAVE-145-18	101.4	101.3	0.2
PAVE-30-59	71.8	70.4	1.4
PAVE-350-14	111.6	113.6	-2.0
PAVE-40-60	70.8	71.5	-0.7
PAVE-450-16	105.8	106.5	-0.7
PAVE-90-51	73.5	74.5	-1.0
RAF	49.2	50.5	-1.3
RAF-110-62	73.8	74.5	-0.7
RAF-170-25	95.9	93.7	2.2
RAF-170-60	74.3	74.7	-0.4
RAF-210-15	118.9	118.2	0.7
RAF-220-18	110.8	111.0	-0.2
RAF-220-31	98.2	97.4	0.8
RAF-295-20	111.3	112.8	-1.5
RAF-340-32	96.0	96.1	-0.1
RAF-460-22	109.9	107.9	2.0
RAF-90-74	70.9	70.5	0.4

Experimental data were simultaneously fitted with Equation 5 and 6 and the CAM model parameters were calculated by using TableCurve 2D software. The CAM model fits the experimental data very well for neat bitumens (RAF, $R^2 = 0.9997$), however the quality of the fit decreased with increased bitumen oxidation (RAF-210-15, $R^2 = 0.9824$). The CAM model was further validated for the black diagram (Figure 4A). The model limitation for the most oxidized samples is apparent and therefore, the model outcomes should be interpreted with caution when applied to these samples.

The CAM model has certain difficulties capturing the high frequency asymptotic modulus value or glassy modulus. No correlation between glassy modulus and severity of oxidation was observed (data not presented). Setting glassy modulus to a constant of 1 GPa for all samples was not considered as glassy modulus is expected to increase with oxidation as a more rigid molecular structure is formed. The rheological index was plotted versus the oxidation time in Figure 4B. The rheological index increased with oxidation time. There seemed not to be any significant difference in R for air blown samples among the same target grade when different feedstocks and oxidation temperatures are applied. The rheological index, R, is in fact a reciprocal value of β and it is somewhat related to Pfeiffer penetration index (temperature susceptibility). Note the correlation between R and PI in Figure 4C, and specifically the difference between neat/air rectified and oxidized samples. This observation should be used with caution as the model was found to be less reliable for the most severely oxidized samples. The rather significant increase in rheological index indicates that the relaxation properties of studied bitumen are impacted by oxidation. As was previously discussed, the increase in rigidity of the molecular backbones due to loss of rotational degree of freedom and an increase in degree of low energy intra-molecular interaction or association due to oxidation significantly reduces the molecular mobility. Molecular mobility is closely related to material relaxation properties. This is best demonstrated in Figure 4D where mean relaxation time is plotted versus oxidation time. The mean relaxation time increased with increased severity of oxidation. The increase was rather dramatic. For example, the samples prepared by air blowing at 260 °C showed that the mean relaxation time increased by an order of magnitude approximately every 17 minutes of air blowing. The adjusting parameter, κ, was found to slightly increase with oxidation time (data not presented).

3.7 Discrete Relaxation and Retardation Spectra

The discrete relaxation and retardation spectra were calculated using a custom Excel® routine based on the approach of Baumgaertel and Winter [18]. It was found that, with increased severity of oxidation, the relaxation and retardation spectra gradually shifted to longer relaxation/retardation times by several orders of magnitude. The shift was most notable in the longest time region (Figure 5AB). Air rectified paving grades which originated from PAVE showed the least deviation from spectra of neat bitumen. This observation is in agreement with previous results obtained by an analysis of the materials functions and CAM model and confirms the large impact of oxidation on bitumen's ability to relax imposed stresses.
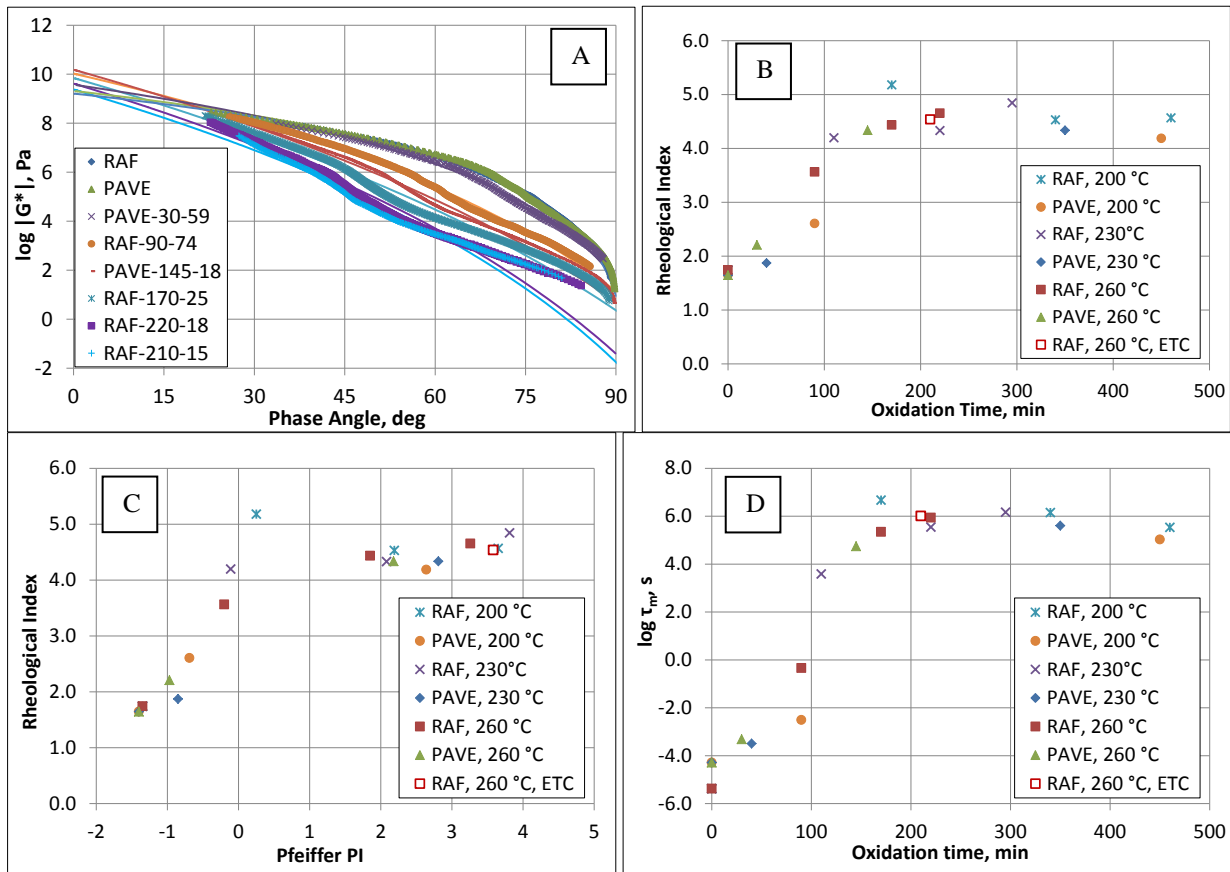

Figure 4. Black diagram, CAM fit (A). Rheological index (CAM model) versus oxidation time (B). Rheological index versus Pfeiffer penetration index (C). Mean relaxation time versus oxidation time (D).
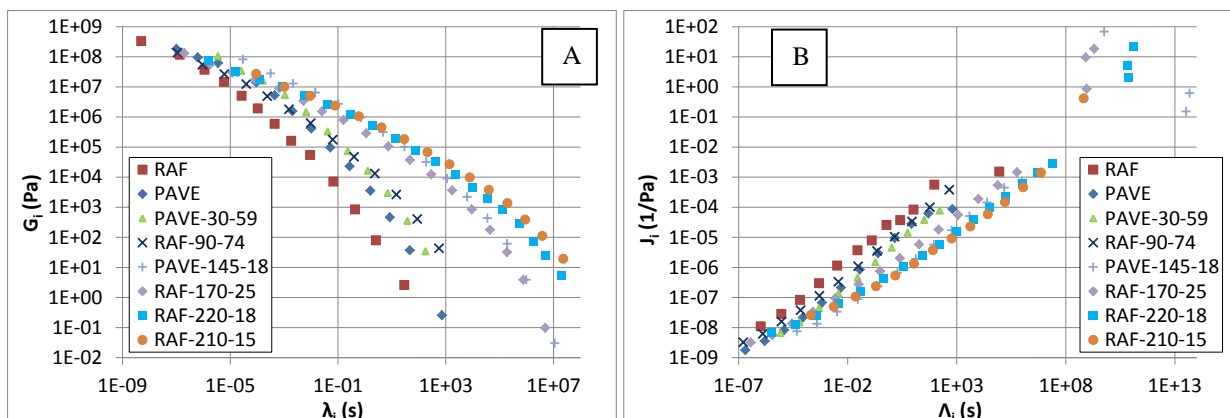

Figure 5. Relaxation spectra (A). Retardation spectra (B).

On a molecular level, stress relaxation and relaxation rate are directly linked to molecular mobility, chain flexibility and the number of degrees of freedom (intra- and inter-molecular). During bitumen oxidation, the molecular mobility is reduced due to the incorporation of multiple bonds. Some of the flexible saturated chains and side-chains are cleaved and evaporated, diminishing their contribution to stress relaxation. The degree of freedom of the single covalent bond is lost by the incorporation of multiple bonds, carbonyl and sulphonyl functional groups, and ring structures. On the nano

scale, the molecular mobility/degree of freedom is reduced by weak intermolecular forces as was already discussed. The results presented here clearly indicated dramatic changes in material relaxation properties during oxidation. This is primarily true in the long relaxation time range. In the short relaxation time range, the difference among samples is less apparent. In addition, the PAVE samples seem to have slightly longer relaxation times than equivalent RAF samples in this range. As the relaxation properties are linked to molecular mobility this confirms the previous observation and can be attributed to lower concentration of saturated light ends in PAVE samples due to PAVE higher distillation temperature.

3.8 Creep Compliance, $J(t)$

Time dependent material functions such as creep compliance and stress relaxation modulus are typically measured in transient experiments (constant stress or strain experiments). These experiments can be very lengthy at lower temperatures where relaxation times become significant. Relaxation or retardation spectra previously calculated from dynamic material functions allow for direct calculation of material functions in the time domain, saving significant experimental effort and offering additional information about the rheological behavior of the material.
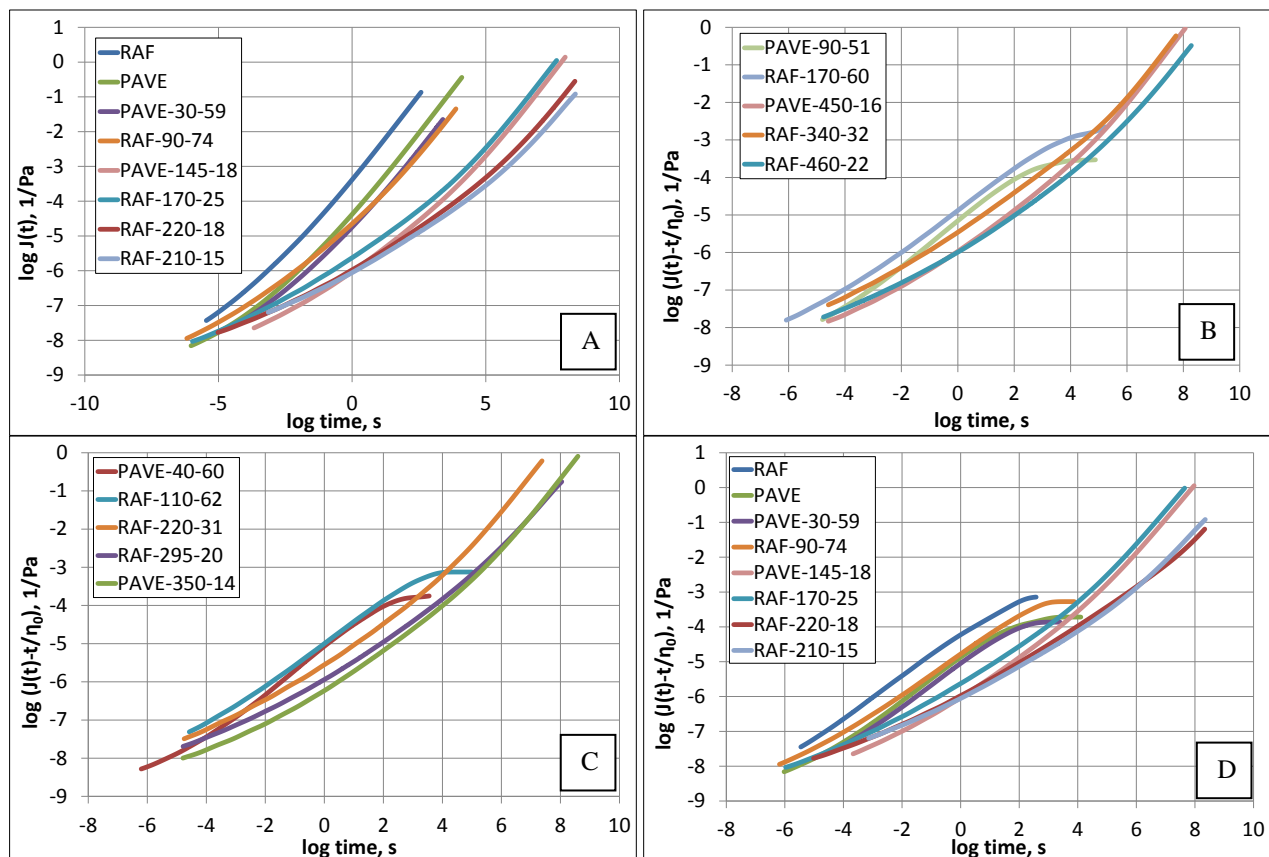

Figure 6. Creep compliance. Samples oxidized at 260 °C (A). Creep compliance minus contribution of viscous flow $J(t) - t/\eta_0$. Samples oxidized at 200 °C (B), at 230 °C (C), at 260 °C (D).

The creep compliance, $J(t)$, can be calculated from discrete retardation spectra by the following relationship:

$$J(t) = J_g + t/\eta_0 + \sum_{i=1}^{N-1} J_i[-\exp(-t/\Lambda_i)] \qquad \textbf{7}$$

where η_0 is the zero shear viscosity, J_g is the instantaneous (glassy) compliance, J_i, Λ_i is the compliance and a retardation time of a Voigt element. Creep compliance was calculated for all samples (Figure 6A). At short times, $J(t)$, gradually approaches a value of ~10^{-9} 1/Pa, which is characteristic of a hard glasslike solid. The corresponding region on the time scale is the glassy zone. The compliance magnitude in the glassy zone relates to an absence of any configurational rearrangements within the observation time, i.e. the molecular chain configurations are immobilized. The samples generated from PAVE show slightly lower values of compliance at very short times. This suggests that the PAVE samples showed a reduced tendency for rearrangements compared to their RAF counterparts. This is consistent with previous observations that the RAF samples contain a higher portion of lighter saturated molecules than PAVE samples. Saturated chains are the last to vitrify on cooling. Therefore, the saturated molecules still enable configurational rearrangement at times shorter than the other bitumen constituents. The degree of oxidation does not

seem to have an effect on this differentiation between RAF and PAVE samples. The saturated fraction is the least chemically altered fraction during bitumen oxidation and therefore it remains present to some extent present in all RAF air blown samples.

At long times, $J(t)$ increases without limit for uncross-linked materials. This was observed for all samples in this study as $J(t)$ also includes a contribution from viscous flow, t/η_0. When the contribution of the viscous flow is subtracted, the remaining quantity $J(t) - t/\eta_0$ may approach a constant equilibrium compliance, J_e, at long time zone as observed in low molecular weight polymers (M_w~11,000 g/mol) at a level of approximately 10^{-4} 1/Pa. In high molecular weight polymers (M_w~300,000 g/mol) limiting equilibrium compliance is not observed and $J(t) - t/\eta_0$ increases without limit as typically the coupling entanglements greatly prolong the time for long-range configurational changes [3]. Straight-run and air-rectified samples showed a limiting value, J_e, as observed in low molecular weight materials. The more oxidized samples, however did not show the limiting value and behaved very much like high molecular weight polymers (Figure 6B-D). The molecular weight of air blown bitumens is lower by at least two orders of a magnitude than molecular weight of high molecular weight polymers [1, 3] and therefore the absence of J_e for more oxidized samples was not expected. In molecular terms, the magnitude of J_e measures average distortion of the polymer coils during flow, when ample time was allowed for Brownian motion and hydrodynamic torques to reach a steady state. The increase in polarity during oxidation may amplify intra- and inter-molecular interactions or forces. Stronger intra- and inter-molecular interactions present in the most oxidized samples may slow down Brownian motion resulting in the formation of a weak structure of a very high apparent molecular weight and may prevent induced longer range molecular rearrangements similar to that observed in high molecular weight polymers. This separation among neat/air rectified and oxidized bitumen behavior as observed in Figure 6B-D correlated well with data presented in Figure 4C.

3.9 Stress Relaxation Modulus, $G(t)$

The relaxation modulus, $G(t)$, can be expressed as a discrete set of exponential decays:

$$G(t) = G_e + \sum_{i=1}^{N} G_i \exp(-t/\lambda_i) \qquad \textbf{8}$$

where G_e is the equilibrium modulus, G_i is the shear rigidity and λ_i is the relaxation time of a Maxwell element. It represents the stress/strain ratio at constant deformation plotted versus time (Figure 7A). The noise observed at longest times in some samples is most likely an artifact of discrete relaxation spectra calculation. The best effort was made to minimize a number of individual elements while achieving a good fit of material functions.

In certain regions, $G(t) \cong 1/J(t)$, and the logarithmic plots nearly appear as mirror images. At short times, $G(t)$ approached a limiting value, called the glassy modulus, $G_g = 1/J_g$, which typically reaches 10^9 Pa and represents the rigidity in absence of backbone rearrangements. This was observed in the samples studied and mirrors the observation already described for creep compliance. At long times, $G(t)$ gradually decreased and eventually vanished in the terminal zone. In terms of the model used, this corresponds to the complete relaxation of all springs. In molecular terms, it corresponds to the resumption of random average configurations by the molecular coils, which have completely freed themselves from constraints imposed on them by deformation. At intermediate times, stress gradually falls as the distortion adjusts itself through Brownian motion. The drop in relaxation modulus takes place in a single stage (note the curve shape in Figure 7A), typical of uncross-linked low molecular weight materials.

3.10   Zero Shear Viscosity (η_0, ZSV)

Zero shear viscosity, η_0, is a viscosity limit at $\dot{\gamma} \to 0$, and thus it represents a time independent material characteristic constant and it is directly related to material chemical composition and internal structure. Zero shear viscosity can be calculated from discrete relaxation spectrum as $\eta_0 = \sum_{i=1}^{N} G_i \lambda_i$. Zero shear viscosity was calculated for studied samples and is presented in Figure 7B. During oxidation η_0 increased dramatically and the increase correlated very well with increased oxidation time. The slope on a semi-log plot can be considered as oxidation rate. This indicates that the process of bitumen oxidation is gradual and there is no change in oxidation mechanism at any stage of the process. As expected, the oxidation rate increased with increased process temperature. The oxidation rate was faster in RAF samples at any given process temperature. Results for ETC BURA III (RAF-210-15) indicated that the ETC oxidizer is more effective in oxidation. It is apparent from Figure 7B, that the SRC oxidizer would need approximately an additional 30 minutes of oxidation time in order to reach the same level of η_0. Bitumen air blowing is a mass transfer

limited process. Despite the oxidation conditions in SRC and ETC oxidizer were nearly identical, higher level of air-bitumen surface area was probably achieved in the ETC oxidizer.
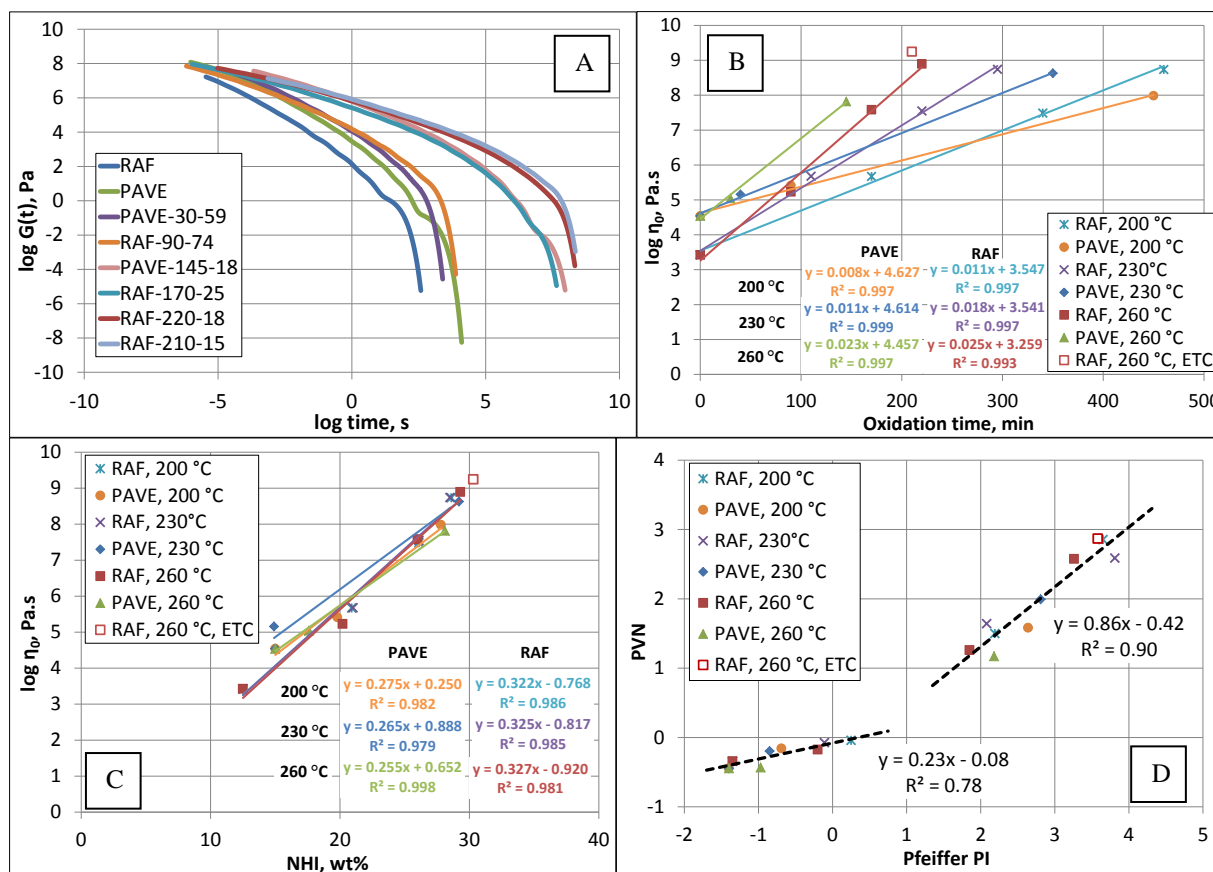

Figure 7. Relaxation modulus (A). Zero shear viscosity versus oxidation time (B). Zero shear viscosity versus NHI (N-Heptane Insolubles) content (C). PVN versus Pfeiffer PI (D).

3.11   Effect of Oxidation Temperature

N-heptane asphaltenes or insolubles, NHI, content increase is often used as an indicator of progressing oxidation. Generally, the more severely (longer or at higher temperature) the bitumen is air blown, the higher the observed asphaltene gain. In order to assess the effect of temperature, semi logarithmic plot of zero shear viscosity (ZSV) versus NHI content is presented (Figure 7C). A linear increase of ZSV with NHI was observed. The slopes are identical irrespective of the oxidation temperature. The rates are faster in RAF confirming slightly higher rates in RAF as discussed above. The chart indicated that the influence of oxidation temperature is minor; the rheological parameter (ZSV) related to composition and structure (both molecular level and macro structure) closely followed the evolution of NHI, which is a solubility parameter related to chemical composition.

3.12   Temperature Susceptibility

Temperature susceptibility typically decreases with increased oxidation. Increase in penetration index, PI, or penetration-viscosity number PVN [19], is traditionally a good indicator of oxidation progression. A plot of PVN versus PI is offered in Figure 7D as an alternative to the plot presented in Figure 4C to separate neat/air rectified and oxidized asphalts. This plot indicates a difference in the ratio of softening point to viscosity at 135 °C between neat/air rectified and oxidized samples. The same separation was observed in log ZSV versus softening point plot (not presented) and also in the equilibrium compliance plot presented in Figure 6B-D. The empirically derived rheological parameters used to describe temperature susceptibility are closely related to rheological parameters derived from mastercurves.

4. CONCLUSIONS

In order to understand the impact of oxidation on bitumen rheological properties, neat, air rectified and oxidized bitumen were subjected to a series of dynamic oscillatory tests. Mastercurves of dynamic material functions were constructed and analyzed. Discrete relaxation and retardation spectra were calculated and relaxation modulus and creep compliance were derived. Results showed that oxidation caused the storage and loss moduli to increase and phase angle to decrease at a given frequency, indicating an increase in material elasticity. Relaxation spectra were progressively shifted to longer relaxation times with increased severity oxidation. The changes in rheological properties during

oxidation were explained in molecular terms. It was shown that oxidation on the molecular level leads to increased rigidity of molecular structures, reduced molecular mobility and increased molecular association tendencies.

To differentiate between the air rectified paving grades and oxidized roofing grades, the black diagram was analyzed. The air rectified samples did not differ from neat bitumen, suggesting that the oxidation did not significantly alter the composition of these samples. With increased oxidation severity, however, the black diagram showed clear distinctions versus neat asphalts. The oxidation time at a given temperature was found to be the most important factor influencing the curve shape progression in the black diagram, while feedstock penetration does not seem to be a factor.

When creep compliance was corrected for contribution from viscous flow, the limiting equilibrium compliance was observed at long times for neat and air rectified paving grades, but not for oxidized roofing grades. This was attributed to high polarity (lower solubility) of asphalt molecules in oxidized samples. Higher tendency to form molecular aggregates or to interact through weak intermolecular forces may lead to increased apparent molecular weight and further reduce molecular mobility. When rheological index or penetration viscosity number were plotted versus penetration index, the same separation between neat/air rectified and oxidized samples was observed.

All samples analyzed in this study originated from a single crude oil and results presented here need to be validated for a larger variety of feedstocks. Nevertheless, it is shown that detailed rheology can identify the progress or severity of oxidation of bitumen. The oxidation severity is closely related to oxidation time at a given temperature, and not much to feedstock penetration. When samples were oxidized to a common softening point target at different temperatures, the oxidation temperature seemed not to be a significant factor when these products are compared. It was also shown that traditionally used parameters such as penetration index or penetration viscosity number correlate to scientific parameters derived from rheological data when severity of bitumen oxidation is considered.

Future work is suggested to focus on correlating the findings observed in rheological testing with changes at the molecular level. Nuclear magnetic resonance and Fourier transformed infrared spectroscopy can be deployed to study increase in molecular structure rigidity. Modulated differential scanning calorimetry can help to identify the changes in bitumen glass transition and physical ageing which are closely related to molecular mobility [20].

REFERENCES

[1]   Petersen, J. C., A Review of the Fundamentals of Asphalt Oxidation, Trans Res Board,Washington, D.C., 2009.
[2]   Pfeiffer, J. -P., van Doormaal, P. M. The Rheological Properties of Asphaltic Bitumens. Journal of the Institution of Petroleum Technologists, 22, 414-440, 1936.
[3]   Ferry, J. D., Viscoelastic Properties of Polymers, 3rd ed., Wiley, New York, 1980.
[4]   Huynh, H. K., et al., Effect of Molecular-Weight and Composition on Glass Transition Temperatures of Asphalts, Anal Chem, 50(7), 976-979, 1978.
[5]   Weyland, H. G., Hoftyzer, P. J., & Krevelen, D. W., Prediction of the Glass Transition Temperature of Polymers, Polymer, 11(2), 79-87, 1970.
[6]   Krevelen, D. W., Hoftyzer, P. H., Properties of Polymers, Their Estimation and Correlation With Chemical Structure, Elsevier Scientific Pub. Co., Amsterdam, 1976.
[7]   Petersen, J. C., Quantitative Functional Group Analysis of Asphalts Using Differential Infrared Spectroscopy and Selective Chemical Reactions - Theory and Application, Trans Res Rec, 1096, 1-11, 1986.
[8]   Moschopedis, S. E., Speight, J. G., Investigation of Hydrogen Bonding by Oxygen Functions in Athabasca Bitumen. Fuel, 55(3), 187-192, 1976.
[9]   Park, S. J., Mansoori, G. A., Aggregation of Heavy Organics in Petroleum Crudes, Energ Source, 10(2), 109-125, 1988.
[10]   Murgich, J., Intermolecular Forces in Aggregates of Asphaltenes and Resins, Pet Sci Technol, 20(9-10), 983-997, 2002.
[11]   Juyal, P., Merino-Garcia, D., Andersen, S. I., Effect on Molecular Interactions of Chemical Alteration of Petroleum Asphaltenes. I. Energ Fuel, 19(4), 1272-1281, 2005.
[12]   Merino-Garcia, D., Andersen, S. I., Interaction of Asphaltenes With Nonylphenol by Microcalorimetry, 20(4), 1473-1480, 2004.
[13]   Israelachvili, J. N., Intermolecular and Surface Forces With Applications to Colloidal and Biological Systems, Academic Press, London, 1985.
[14]   Kriz, P., Glass Transition and Physical Hardening of Asphalts, PhD Thesis, University of Calgary, 2009.
[15]   Williams, M. L., Landel, L. F., Ferry, J. D., The Temperature Dependence of Relaxation Mechanisms in Amorphous Polymers and Other Glass-Forming Liquids, J Am Chem Soc, 77(14), 3701-3707, 1955.
[16]   Christensen, D. W., Anderson, D. A., Interpretation of Dynamic Mechanical Test Data for Paving Grade Asphalt, Association of Asphalt Paving Technologists, 61, White Bear Lake, Minn., 67-116, 1992.
[17]   Marasteanu, M. O., Anderson, D. A., Improved Model for Bitumen Rheological Characterization, Eurobitume Workshop on Performance Related Properties for Bituminous Binders, Eurobitume, Brussels, 1999.
[18]   Baumgaertel, M., Winter, H. H., Determination of Discrete Relaxation and Retardation Time Spectra from Dynamic Mechanical Data, Rheol. Acta, 28, 511-519, 1989.
[19]   McLeod, N. W., Using Paving Asphalt Rheology to Impair or Improve Asphalt Pavement Design and Performance, in O. E. Briscoe, Asphalt Rheology: Relationship to Mixture, ASTM STP 941, ASTM, Philadelphia, 51-75, 1987.
[20]   Kriz, P., Stastna, J., Zanzotto, L., Glass Transition and Phase Stability in Asphalt Binders, Road Materials and Pavement Design, 9, 37-65, 2008.